medRxiv preprint doi: https://doi.org/10.1101/2024.05.15.24307407; this version posted May 15, 2024. The copyright holder for this preprint (which was not certified by peer review) is the author/funder, who has granted medRxiv a license to display the preprint in perpetuity. It is made available under a CC-BY-NC-ND 4.0 International license .

Radiomic based investigation of a potential link between precuneus and fusiform gyrus with Alzheimer's disease

Simran Sharma[1], Kavita Kundal[1], Ishsirjan Kaur Chandok[1], Neeraj Kumar[1, 2*], Rahul Kumar[1*]

[1]Department of Biotechnology, Indian Institute of Technology Hyderabad, Kandi, Telangana 502284, India

[2]Department of Liberal Arts, Indian Institute of Technology Hyderabad, Kandi, Telangana 502284, India

*Correspondence: rahulk@bt.iith.ac.in; neeraj.kumar@la.iith.ac.in

Abstract

Alzheimer's disease (AD) is acknowledged as one of the most common types of dementia. Various brain regions were found to associated with AD pathology. Precuneus and fusiform gyrus are two notable regions whose role has been implicated in cognitive function. However, a thorough investigation was lacking to link these regions with AD pathology. In this study, we conducted a comprehensive radiomic based investigation using magnetic resonance imaging (MRI) scans to link precuneus and fusiform gyrus with AD pathology. We obtained T1 weighted MR scans of AD (n=133), MCI (n=311) and CN (n=195) subjects from ADNI database at three different time points (i.e., 0, 6 and 12 months). Then, we conducted statistical analysis to compare these features among AD, MCI and CN subjects. We found significant decline in gray matter volume (GMV) and cortical thickness of both precuneus and fusiform gyrus in AD as compared to the MCI and CN subjects. Further, we utilized these features to develop machine learning classifiers to classify AD from MCI and CN subjects and achieved accuracy of 97.78% and 94.41% respectively. These results strengthen the connection of precuneus and fusiform gyrus with AD pathology and opens a new avenue of AD research.

NOTE: This preprint reports new research that has not been certified by peer review and should not be used to guide clinical practice.

medRxiv preprint doi: https://doi.org/10.1101/2024.05.15.24307407; this version posted May 15, 2024. The copyright holder for this preprint (which was not certified by peer review) is the author/funder, who has granted medRxiv a license to display the preprint in perpetuity. It is made available under a CC-BY-NC-ND 4.0 International license .

1. Introduction

Alzheimer's disease (AD) is the primary cause of dementia, affecting 60% to 80% of cases globally (1). It's characterized by memory loss, cognitive decline, and behavioral changes, leading to a loss of independence (1). Mild cognitive impairment (MCI) is a transitional stage, with about 35% of cases progressing to AD or dementia within 3-4 years (1). In 2015, AD cost around 818 billion USD globally, impacting over 47 million individuals (2). By 2050, its prevalence is projected to quadruple, affecting nearly 1 in 85 people, primarily due to population aging (3).

In Alzheimer's Disease (AD), the precuneus and fusiform gyrus are pivotal regions implicated in the neurodegenerative cascade leading to cognitive impairment and functional decline. The precuneus serves as a central hub for various cognitive processes, including episodic memory retrieval, visuospatial processing, and self-referential cognition (4, 5, 6, 7, 8). Numerous neuroimaging studies have consistently revealed significant atrophy, hypometabolism within the precuneus, and reduced connectivity with the default mode network in individuals with AD (9, 10, 11, 12,13,14) particularly in the early stages of the disease (15). The atrophy in the precuneus area is also shown even in the non-amnestic Aβneg-AD individuals (16).

Conversely, the fusiform gyrus is renowned for its specialization in facial recognition and the processing of complex visual stimuli (17). In AD, alterations in the fusiform gyrus have been observed as reduced gray matter volume (18) and disrupted functional connectivity (19). These changes underlie the characteristic deficits in facial recognition and discrimination encountered by AD patients, contributing to their impaired social cognition and interpersonal interactions.

Emerging evidence suggests that the precuneus serves as a convergence zone integrating sensory, mnemonic, and attentional information critical for cognitive processing, including facial recognition mediated by the fusiform gyrus (20, 21, 22, 23 ,7). Disruptions within this network, specifically in face perception, may lead to the cascade of cognitive impairments like disruption in face-related episodic memory retrieval, limited interpersonal relations, and poor spatial awareness observed in AD, encompassing deficits in memory consolidation, attentional control, and social cognition. Understanding of the structural and functional alterations within these regions may offer valuable biomarkers for early diagnosis and monitoring disease progression in AD. The present study employs a machine learning-based approach

medRxiv preprint doi: https://doi.org/10.1101/2024.05.15.24307407; this version posted May 15, 2024. The copyright holder for this preprint (which was not certified by peer review) is the author/funder, who has granted medRxiv a license to display the preprint in perpetuity. It is made available under a CC-BY-NC-ND 4.0 International license .

leveraging radiomics analysis of MRI data to identify novel biomarkers from the precuneus and fusiform gyrus by systematically analyzing volumetric and surface features extracted from MRI images of individuals across different stages of cognitive impairment, including cognitively normal (CN), mild cognitive impairment (MCI), and AD. We have developed an ML-based classifier that can categorize individuals into MCI or AD based on their precuneus and fusiform gyrus features.

2. Methodology

2.1 Data Description

We downloaded the T1-weighted MRI images from the ADNI1 collection (named ADNI1: Complete 1Yr 1.5T) in the Alzheimer's Disease Neuroimaging Initiative (ADNI) database (http://adni.loni.usc.edu/), which comprises cohorts with 195 cognitive normal (CN), 311 mild cognitive impairment (MCI), and 133 Alzheimer's disease (AD) subjects. The age range for CN individuals spans from 60 to 91 years while those with MCI range from 55 to 91 years, and for those diagnosed with AD, it ranges from 55 to 90 years. In the ADNI dataset, Mini-Mental State Examination (MMSE), Clinical Dementia Rating (CDR), and the National Institute of Neurological and Communicative Disorders and Stroke/Alzheimer's Disease and Related Disorders Association (NINCDS/ADRDA, 24) were the criteria used to assess the level of cognition in the samples (CN, MCI, and AD) (https://adni.loni.usc.edu/methods/documents/). CNs have an MMSE score in the range of 24–30, a CDR score of 0, and no signs of depression. MCIs have an MMSE score in the range of 24–30 and a CDR score of 0.5, with memory complaints and minimally impaired daily activities. AD criteria include MMSE scores of 20–26 (inclusive) and a CDR of 0.5 or 1.0, fulfilling NINCDS/ADRDA criteria (https://adni.loni.usc.edu/methods/documents/). For each subject, three time points of scans were available, i.e., the initial screening (month 0), the 6-month mark (month 06), and the 12-month mark (month 12). The MRI 1.5T images were acquired with multicoil phased-array head coil (MA), FOV set at 240 x 240 mm, flip angle of 8 degrees, and TR of 2300 ms (25). In the ADNI collection, images were pre-processed for multi-planar reconstruction-reslicing (MPR-R), B1 radiofrequency pulse for non-uniformity correction, gradient warping, and N3 to reduce intensity non-uniformity (https://adni.loni.usc.edu/methods/documents/).

medRxiv preprint doi: https://doi.org/10.1101/2024.05.15.24307407; this version posted May 15, 2024. The copyright holder for this preprint (which was not certified by peer review) is the author/funder, who has granted medRxiv a license to display the preprint in perpetuity. It is made available under a CC-BY-NC-ND 4.0 International license .

2.2 Radiomic-Based Feature Extraction and Statistical Method

We implemented the fully automated 'Recon-All' pipeline provided by Freesurfer software (http://surfer.nmr.mgh.harvard.edu/) for feature extraction. It is an open-source package to analyze and display structural, functional, and diffusion neuroimaging data from cross-sectional and longitudinal research (https://surfer.nmr.mgh.harvard.edu/). This pipeline initially follows a few image processing steps, i.e., motion artifact correction, transformation to Talairach image space, intensity normalization, and skull striping (26). Cortical parcellation was performed for feature extraction using the Desikan-Killiany atlas, which divides the MRI scans into discrete 34 anatomical regions (27). Eight different types of radiomic features i.e., the total gray matter volume (GMV, mm^3), the number of vertices, the average cortical thickness (mm), the total surface areas (mm^2), the integrated rectified mean curvature (mm^-1), the integrated rectified Gaussian curvature (mm^-2), the folding index, and the intrinsic curvature index) were calculated for the precuneus and fusiform gyrus from both left and right hemisphere.

We applied the nonparametric Mann-Whitney U test to compare these eight features of the precuneus and fusiform gyrus between CN, MCI, and AD subjects at three time points. The p-values were adjusted using the Benjamin-Hochberg correction method. Box and whisker plots were used to provide a graphical representation of the distribution of these groups.

2.3 Machine Learning Predictive Model Development

We combined above mentioned 16 radiomic features of both right and left hemispheres of precuneus and fusiform gyrus (total 32 features) and trained three binary classification models, i.e., AD vs CN, MCI vs AD, and CN vs MCI. We also used age of the individuals as one of the features to see its impact on the performance of these models. Additionally, classification models that solely used precuneus or fusiform-based features were also constructed.-We deployed the Random Forest Classifier (RFC) algorithm to develop the classification models. First, the dataset was divided into a training dataset (80%) and a test dataset (20%), and the KNN imputation method was implemented to ensure uniformity (28). The class imbalance was addressed through random undersampling, while hyperparameter optimization of the RFC was carried out

medRxiv preprint doi: https://doi.org/10.1101/2024.05.15.24307407; this version posted May 15, 2024. The copyright holder for this preprint (which was not certified by peer review) is the author/funder, who has granted medRxiv a license to display the preprint in perpetuity. It is made available under a CC-BY-NC-ND 4.0 International license .

using the "RandomizedSearchCV" function to enhance model performance. The trained model underwent a comprehensive performance evaluation using various statistical metrics, e.g., accuracy, precision, recall, F1-score, ROC AUC, and Matthews Correlation Coefficient (MCC) (29, 30,1). Further, all the classifier models were tested on a test dataset to select the top-performing model.

3. Results

3.1 Statistical Analysis for MRI-based Radiomic Features

We extracted the volumetric and surface related features from MRI images and applied Mann-Whitney U test to compare the eight classes of these radiomic features of precuneus and fusiform gyrus (Supplementary Tables 1-8 and Supplementary Figures 1-7). Among these features, we found significant reduction in gray matter volume (GMV) of precuneus among AD patients as compared to the MCI ($P_{adjusted}$ = 1.95e-05) and CN ($P_{adjusted}$ = 8.78e-09) at 0 time point (Figure 2 and Supplementary Table 1). Similar trends were observed at six- and twelve-months follow-ups (Figure 2 and Supplementary Table 1). Interestingly, the GMV of the fusiform gyrus was also significantly reduced in the AD patients as compared to the MCI ($P_{adjusted}$ = 3.50e-06) and CN ($P_{adjusted}$ = 2.66e-09) at 0 time point (Figure 3 and Supplementary Table 1). At time points of 6 and 12 months also, reduction in GMV of fusiform gyrus was observed (Figure 3 and Supplementary Table 1). In addition to GMV, we also observed significant reduction in average cortical thickness in both precuneus and fusiform gyrus (Supplementary Table 2 and Supplementary Figure 1) and increase in gaussian and mean curvature of fusiform gyrus (Supplementary Tables 3 and 4 and Supplementary Figures 2 and 3). We also performed statistical analysis for other radiomic features and observed significant differences (Supplementary Tables 4-8 and Supplementary Figures 4-7).

3.2 Performance of Machine Learning-based Classification Models

We developed three classification models in this study i.e., AD vs CN, MCI vs AD and MCI vs CN and obtained an adequate performance for all three models using RFC. For AD vs CN (33 features), we obtained accuracy of 97.78% and 93.25% with AUC values of 0.98 and 0.97 in training and test dataset respectively (Table 1 and Figure 4(a)). For AD vs MCI (33 features), we obtained accuracy of 94.41% and 82.70% with AUC

medRxiv preprint doi: https://doi.org/10.1101/2024.05.15.24307407; this version posted May 15, 2024. The copyright holder for this preprint (which was not certified by peer review) is the author/funder, who has granted medRxiv a license to display the preprint in perpetuity. It is made available under a CC-BY-NC-ND 4.0 International license .

values of 0.96 and 0.92 in training and test dataset respectively (Table 2 and Figure 4(b)). For MCI vs CN (33 features), we obtained accuracy of 96.56% and 86.26% with AUC values of 0.97 and 0.94 in training and test dataset respectively (Table 3 and Figure 4(c)). To mitigate the effect of age on model performance, we checked the performance of these models without age as one of the training features. Strikingly, without age (32 features) also, we observed the adequate performance for all three models (Tables 1-3 and Figure 4) which shows the predictive power of the MRI-based radiomic features of precuneus and fusiform gyrus. Along with accuracy and AUC, we also calculated other statistical matrices to assess the performances of these models (Tables 1-3 and Figure 4). Along with combined models of precuneus and fusiform gyrus, we developed classifier models using radiomic features of either precuneus or fusiform gyrus and found slightly better performance for fusiform gyrus-based classification models (Supplementary Tables 9-14 and Supplementary Figures 8-9).

4. Discussion

In this study, we investigated a potential link between the precuneus and fusiform gyrus with AD pathology using statistical and machine learning analysis on MRI-based radiomic features. We extracted eight MRI-based radiomic features of the left and right hemispheres of the precuneus and fusiform gyrus i.e., gray matter volume, average thickness, folding index, intrinsic curvature index, integrated rectified Gaussian curvature, integrated rectified mean curvature, surface area, and number of vertices using Freesurfer automated pipeline. In our statistical analysis, we observed that gray matter volume of both precuneus and fusiform significantly decreased in AD patients as compared to the MCI and CN at all three time points (0, 6 and 12 months).

Reduced gray matter volume is a prevalent sign of AD pathology and has been proposed as an essential physiological structure of cognitive function decline (31). Our observation aligns with a previous report on Voxel-based research that found gray matter volume reductions in the right fusiform gyrus of AD patients (32). Moreover, lower gray matter density in the precuneus and its atrophy was shown to be more prominent in early-onset AD patients in various voxel-based investigations on gray matter atrophy (15, 33). Additionally, we also observed a significant decrease in average thickness of precuneus and fusiform in AD patients. There was significant increase in gaussian curvature of AD subjects in fusiform gyrus. Significant reduction

medRxiv preprint doi: https://doi.org/10.1101/2024.05.15.24307407; this version posted May 15, 2024. The copyright holder for this preprint (which was not certified by peer review) is the author/funder, who has granted medRxiv a license to display the preprint in perpetuity. It is made available under a CC-BY-NC-ND 4.0 International license .

in cortical thickness was previously reported in patients with AD and MCI (32), however increased gaussian curvature along with a decrease in precuneus and fusiform thickness were not reported earlier. Our findings strengthen the previously identified association between fusiform gyrus and AD pathology and open a new direction of association of precuneus and fusiform gyrus, and AD pathology.

To further investigate the potential of the precuneus and fusiform in classifying AD patients with MCI and CN, we developed random forest-based classifier models. Three binary models were built combining the radiomic features of the precuneus and fusiform gyrus (33 radiomic features including age) and we achieved accuracy of 97.78%. 94.41% and 96.56% for AD vs CN, AD vs MCI and MCI vs CN respectively. Similarly, we also developed classifier without age to mitigate the pervasive nature of age in classifying AD patients from MCI and CN subjects. Without age as a feature, we obtained accuracy of 97.35%, 94.18% and 97.25% for AD vs CN, AD vs MCI and MCI vs CN respectively. These performance metrices of classifier models suggest the classifying potential of radiomic features of precuneus and fusiform gyrus and provide strong evidence for the critical roles of the precuneus and fusiform gyrus in AD pathology. Based on the results of this study, we advocate to study AD pathology in the light of radiomic features of precuneus and fusiform gyrus. However, more investigations are necessary to expand the knowledge and understanding of the precise pathways through which the precuneus and fusiform gyrus contribute to the AD pathology. A better understanding of the role of the precuneus and fusiform gyrus and features based analysis in AD and also non-amnestic Aβneg-AD individuals could provide a generalized early detection method.

In conclusion, this study for the first time providing the evidence-based genesis of roles of both the precuneus and fusiform gyrus combined in AD pathology. Moreover, it adds to the corpus of our knowledge on neuroanatomical foundations of AD and hold significant promise for early detection, prevention, and focused interventions for AD diagnosis and treatment.

5. References

1. Marcisz A, Polanska J. Can T1-Weighted Magnetic Resonance Imaging Significantly Improve Mini-Mental State Examination-Based Distinguishing Between Mild Cognitive Impairment and

medRxiv preprint doi: https://doi.org/10.1101/2024.05.15.24307407; this version posted May 15, 2024. The copyright holder for this preprint (which was not certified by peer review) is the author/funder, who has granted medRxiv a license to display the preprint in perpetuity. It is made available under a CC-BY-NC-ND 4.0 International license .

Early-Stage Alzheimer's Disease? *J Alzheimers Dis*. 2023;92(3):941-957. doi:10.3233/JAD-220806

2. Cai JH, He Y, Zhong XL, et al. Special Review Magnetic Resonance Texture Analysis in Alzheimer's disease. Published online 2020. doi:10.1016/j.acra.2020.01.006
3. Chaddad A, Desrosiers C, Niazi T. Deep Radiomic Analysis of MRI Related to Alzheimer's Disease. *IEEE Access*. 2018;6:58213-58221. doi:10.1109/ACCESS.2018.2871977
4. Cavanna AE, Trimble MR. The precuneus: a review of its functional anatomy and behavioural correlates. *Brain*. 2006;129(Pt 3):564-583. doi:10.1093/BRAIN/AWL004
5. Wagner AD, Shannon BJ, Kahn I, Buckner RL. Parietal lobe contributions to episodic memory retrieval. *Trends Cogn Sci*. 2005;9(9):445-453. doi:10.1016/J.TICS.2005.07.001
6. Mazzoni G, Clark A, De Bartolo A, et al. Brain activation in highly superior autobiographical memory: The role of the precuneus in the autobiographical memory retrieval network. *Cortex*. 2019;120:588-602. doi:10.1016/J.CORTEX.2019.02.020
7. Frings L, Wagner K, Quiske A, et al. Precuneus is involved in allocentric spatial location encoding and recognition. *Exp Brain Res*. 2006;173(4):661-672. doi:10.1007/S00221-006-0408-8
8. Freton M, Lemogne C, Bergouignan L, Delaveau P, Lehéricy S, Fossati P. The eye of the self: Precuneus volume and visual perspective during autobiographical memory retrieval. *Brain Struct Funct*. 2014;219(3):959-968. doi:10.1007/S00429-013-0546-2
9. Buckner RL, Snyder AZ, Shannon BJ, et al. Molecular, Structural, and Functional Characterization of Alzheimer's Disease: Evidence for a Relationship between Default Activity, Amyloid, and Memory. *Journal of Neuroscience*. 2005;25(34):7709-7717. doi:10.1523/JNEUROSCI.2177-05.2005
10. Bailly M, Destrieux C, Hommet C, et al. Precuneus and Cingulate Cortex Atrophy and Hypometabolism in Patients with Alzheimer's Disease and Mild Cognitive Impairment: MRI and 18F-FDG PET Quantitative Analysis Using FreeSurfer. *Biomed Res Int*. 2015;2015. doi:10.1155/2015/583931
11. Desikan RS, Cabral HJ, Hess CP, et al. Automated MRI measures identify individuals with mild cognitive impairment and Alzheimers disease. *Brain*. 2009;132(8):2048-2057. doi:10.1093/BRAIN/AWP123
12. Klaassens BL, van Gerven JMA, van der Grond J, de Vos F, Möller C, Rombouts SARB. Diminished posterior precuneus connectivity with the default mode network differentiates normal aging from Alzheimer's Disease. *Front Aging Neurosci*. 2017;9(APR):97. doi:10.3389/FNAGI.2017.00097/FULL
13. Yokoi T, Watanabe H, Yamaguchi H, et al. Involvement of the precuneus/posterior cingulate cortex is significant for the development of Alzheimer's disease: A PET (THK5351, PiB) and resting fMRI study. *Front Aging Neurosci*. 2018;10(OCT):304. doi:10.3389/FNAGI.2018.00304
14. Desikan RS, Cabral HJ, Fischl B, et al. Temporoparietal MR imaging measures of atrophy in subjects with mild cognitive impairment that predict subsequent diagnosis of Alzheimer disease. *AJNR Am J Neuroradiol*. 2009;30(3):532-538. doi:10.3174/AJNR.A1397
15. Karas G, Scheltens P, Rombouts S, et al. Precuneus atrophy in early-onset Alzheimer's disease: A morphometric structural MRI study. *Neuroradiology*. 2007;49(12):967-976. doi:10.1007/S00234-007-0269-2
16. Chételat G, Ossenkoppele R, Villemagne VL, et al. Atrophy, hypometabolism and clinical trajectories in patients with amyloid-negative Alzheimer's disease. *Brain*. 2016;139(9):2528. doi:10.1093/BRAIN/AWW159

medRxiv preprint doi: https://doi.org/10.1101/2024.05.15.24307407; this version posted May 15, 2024. The copyright holder for this preprint (which was not certified by peer review) is the author/funder, who has granted medRxiv a license to display the preprint in perpetuity. It is made available under a CC-BY-NC-ND 4.0 International license .

17. Kuskowski MA, Pardo J V. The role of the fusiform gyrus in successful encoding of face stimuli. *Neuroimage*. 1999;9(6 I):599-610. doi:10.1006/NIMG.1999.0442
18. Chang YT, Huang CW, Chen NC, et al. Hippocampal amyloid burden with downstream fusiform gyrus atrophy correlate with face matching task scores in early stage Alzheimer's disease. *Front Aging Neurosci*. 2016;8(JUN):197375. doi:10.3389/FNAGI.2016.00145/BIBTEX
19. Cai S, Chong T, Zhang Y, et al. Altered Functional Connectivity of Fusiform Gyrus in Subjects with Amnestic Mild Cognitive Impairment: A Resting-State fMRI Study. *Front Hum Neurosci*. 2015;9(AUGUST). doi:10.3389/FNHUM.2015.00471
20. Dadario NB, Sughrue ME. The functional role of the precuneus. *Brain*. 2023;146(9):3598-3607. doi:10.1093/BRAIN/AWAD181
21. Bogler C, Zangrossi A, Miller C, Sartori G, Haynes JD. Have you been there before? Decoding recognition of spatial scenes from fMRI signals in precuneus. *Hum Brain Mapp*. 2024;45(7):e26690. doi:10.1002/HBM.26690
22. Lee TMC, Leung MK, Lee TMY, Raine A, Chan CCH. I want to lie about not knowing you, but my precuneus refuses to cooperate. *Scientific Reports 2013 3:1*. 2013;3(1):1-5. doi:10.1038/srep01636
23. Platek SM, Wathne K, Tierney NG, Thomson JW. Neural correlates of self-face recognition: An effect-location meta-analysis. *Brain Res*. 2008;1232:173-184. doi:10.1016/J.BRAINRES.2008.07.010
24. McKhann G, Drachman D, Folstein M, Katzman R, Price D, Stadlan EM. Clinical diagnosis of alzheimer's disease: Report of the NINCDS-ADRDA work group⋆ under the auspices of department of health and human services task force on alzheimer's disease. *Neurology*. 1984;34(7):939-944. doi:10.1212/WNL.34.7.939
25. Jack CR, Bernstein MA, Fox NC, et al. The Alzheimer's disease neuroimaging initiative (ADNI): MRI methods. *Journal of Magnetic Resonance Imaging*. 2008;27(4):685-691. doi:10.1002/JMRI.21049
26. Gupta Y, Lee KH, Choi KY, Lee JJ, Kim BC, Kwon GR. Alzheimer's Disease Diagnosis Based on Cortical and Subcortical Features. *J Healthc Eng*. 2019;2019. doi:10.1155/2019/2492719
27. Desikan RS, Ségonne F, Fischl B, et al. An automated labeling system for subdividing the human cerebral cortex on MRI scans into gyral based regions of interest. *Neuroimage*. 2006;31(3):968-980. doi:10.1016/j.neuroimage.2006.01.021
28. Bloch L, Friedrich CM. Classification of Alzheimer's Disease using volumetric features of multiple MRI scans. *Proceedings of the Annual International Conference of the IEEE Engineering in Medicine and Biology Society, EMBS*. Published online July 1, 2019:2396-2401. doi:10.1109/EMBC.2019.8857188
29. Diogo VS, Ferreira HA, Prata D. Early diagnosis of Alzheimer's disease using machine learning: a multi-diagnostic, generalizable approach. *Alzheimers Res Ther*. 2022;14(1). doi:10.1186/S13195-022-01047-Y
30. Basher A, Kim BC, Lee KH, Jung HY. Volumetric Feature-Based Alzheimer's Disease Diagnosis From sMRI Data Using a Convolutional Neural Network and a Deep Neural Network. *IEEEA*. 2021;9:29870-29882. doi:10.1109/ACCESS.2021.3059658
31. Wu Z, Peng Y, Hong M, Zhang Y. Gray Matter Deterioration Pattern During Alzheimer's Disease Progression: A Regions-of-Interest Based Surface Morphometry Study. *Front Aging Neurosci*. 2021;13:593898. doi:10.3389/FNAGI.2021.593898/BIBTEX
32. Wang WY, Yu JT, Liu Y, et al. Voxel-based meta-analysis of grey matter changes in Alzheimer's disease. *Transl Neurodegener*. 2015;4(1):1-9. doi:10.1186/S40035-015-0027-Z/FIGURES/2

medRxiv preprint doi: https://doi.org/10.1101/2024.05.15.24307407; this version posted May 15, 2024. The copyright holder for this preprint (which was not certified by peer review) is the author/funder, who has granted medRxiv a license to display the preprint in perpetuity. It is made available under a CC-BY-NC-ND 4.0 International license .

33. Möller C, Vrenken H, Jiskoot L, et al. Different patterns of gray matter atrophy in early- and late-onset Alzheimer's disease. *Neurobiol Aging*. 2013;34(8):2014-2022. doi:10.1016/J.NEUROBIOLAGING.2013.02.013

6. Acknowledgments

Authors acknowledge the ADNI for providing the clinical and MRI datasets. Authors acknowledge the research infrastructure provided by the Indian Institute of Technology Hyderabad.

7. Conflict of interest

Authors declare no conflict of interest

8. Funding

This work was supported by the seed research grant from the Indian Institute of Technology Hyderabad.

9. Data Availability

All the datasets used in this study are available on ADNI database website (http://adni.loni.usc.edu/).

medRxiv preprint doi: https://doi.org/10.1101/2024.05.15.24307407; this version posted May 15, 2024. The copyright holder for this preprint (which was not certified by peer review) is the author/funder, who has granted medRxiv a license to display the preprint in perpetuity. It is made available under a CC-BY-NC-ND 4.0 International license .

Tables

Table 1: Performance of random forest classifier using radiomic features of both precuneus and fusiform gyrus (left and right hemisphere) for AD vs CN classification (n = Size of Dataset).

Dataset		Accuracy	Precision	Recall	F1- score	AUC	MCC
With Age (33 features)	**Training Dataset (n = 944)**	97.78%	1.00	0.96	0.98	0.98	0.96
	Testing Dataset (n = 237)	93.25%	0.96	0.93	0.94	0.97	0.86
Without Age (32 features)	**Training Dataset (n = 944)**	97.35%	1.00	0.96	0.98	0.98	0.95
	Testing Dataset (n = 237)	91.56%	0.93	0.93	0.93	0.96	0.82

Table 2: Performance of random forest classifier using radiomic features of both precuneus and fusiform gyrus (left and right hemisphere) for AD vs MCI classification (n = Size of Dataset).

Dataset		Accuracy	Precision	Recall	F1- score	AUC	MCC
With Age (33 features)	**Training Dataset (n = 1271)**	94.41%	1.00	0.92	0.96	0.96	0.88
	Testing Dataset (n = 318)	82.70%	0.92	0.82	0.87	0.92	0.63
Without Age (32 features)	**Training Dataset (n = 1271)**	94.18%	1.00	0.92	0.96	0.96	0.88
	Testing Dataset (n = 318)	82.70%	0.93	0.82	0.87	0.92	0.63

medRxiv preprint doi: https://doi.org/10.1101/2024.05.15.24307407; this version posted May 15, 2024. The copyright holder for this preprint (which was not certified by peer review) is the author/funder, who has granted medRxiv a license to display the preprint in perpetuity. It is made available under a CC-BY-NC-ND 4.0 International license .

Table 3: Performance of random forest classifier using radiomic features of both precuneus and fusiform gyrus (left and right hemisphere) for MCI vs CN classification (n = Size of Dataset).

Dataset		Accuracy	Precision	Recall	F1- score	AUC	MCC
With Age (33 features)	**Training Dataset (n = 1454)**	96.56%	1.00	0.94	0.97	0.97	0.93
	Testing Dataset (n = 364)	86.26%	0.89	0.88	0.89	0.94	0.71
Without Age (32 features)	**Training Dataset (n = 1454)**	97.25%	1.00	0.96	0.98	0.98	0.94
	Testing Dataset (n = 364)	84.34%	0.89	0.85	0.87	0.93	0.67

medRxiv preprint doi: https://doi.org/10.1101/2024.05.15.24307407; this version posted May 15, 2024. The copyright holder for this preprint (which was not certified by peer review) is the author/funder, who has granted medRxiv a license to display the preprint in perpetuity. It is made available under a CC-BY-NC-ND 4.0 International license .

Figure Legends

Figure 1: Schematic diagram showing the study plan.

Figure 2: MRI scans showing the gray matter volume (GMV) of precuneus (right hemisphere) from representative samples from cognitive normal (CN), mild cognitive impairment (MCI), and Alzheimer's disease (AD) individuals at three time points (months 0, 6, and 12). Bar plots showing the statistical differences in the GMV of precuneus (z = 31.94, MNI coordinate) (*: $p \leq 0.05$; **: $p \leq 0.01$; ***: $p \leq 0.001$; ****: $p \leq 0.0001$).

Figure 3: MRI scans showing the gray matter volume (GMV) of fusiform gyrus (right hemisphere) from representative samples from cognitive normal (CN), mild cognitive impairment (MCI), and Alzheimer's disease (AD) individuals at three time points (months 0, 6, and 12). Bar plots showing the statistical differences in the GMV of precuneus (z = 31.94, MNI coordinate) (*: $p \leq 0.05$; **: $p \leq 0.01$; ***: $p \leq 0.001$; ****: $p \leq 0.0001$; ns: $p > 0.05$).

Figure 4: ROC plots for the different classifier models developed radiomic features of both precuneus and fusiform gyrus, with and without age; (a) AD vs CN (b) AD vs MCI (c) MCI vs CN.

medRxiv preprint doi: https://doi.org/10.1101/2024.05.15.24307407; this version posted May 15, 2024. The copyright holder for this preprint (which was not certified by peer review) is the author/funder, who has granted medRxiv a license to display the preprint in perpetuity. It is made available under a CC-BY-NC-ND 4.0 International license .

Figure 1

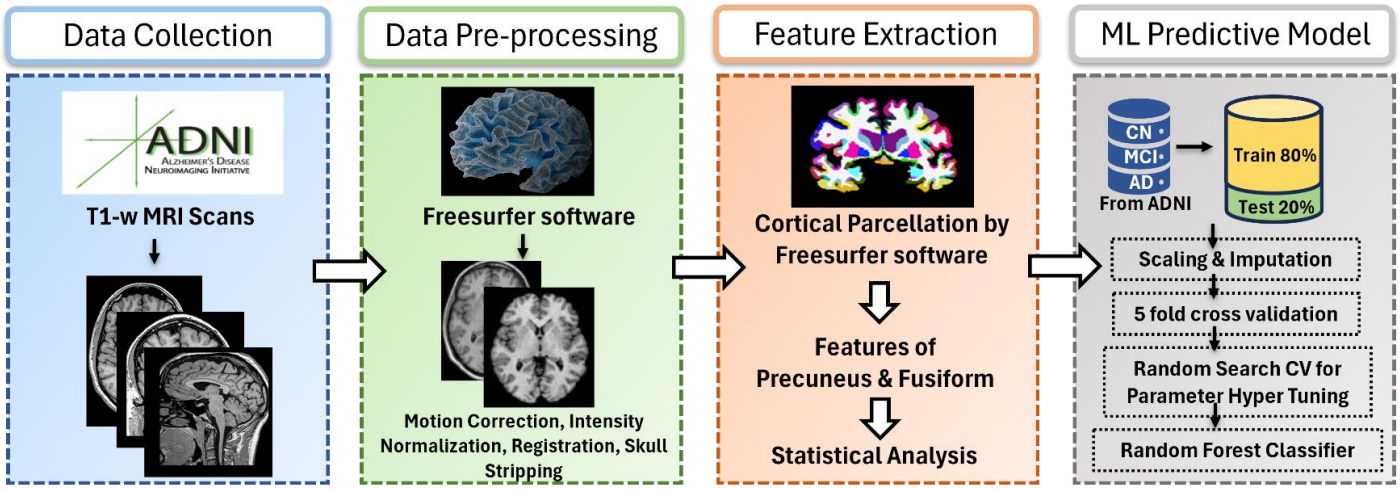

medRxiv preprint doi: https://doi.org/10.1101/2024.05.15.24307407; this version posted May 15, 2024. The copyright holder for this preprint (which was not certified by peer review) is the author/funder, who has granted medRxiv a license to display the preprint in perpetuity. It is made available under a CC-BY-NC-ND 4.0 International license .

Figure 2

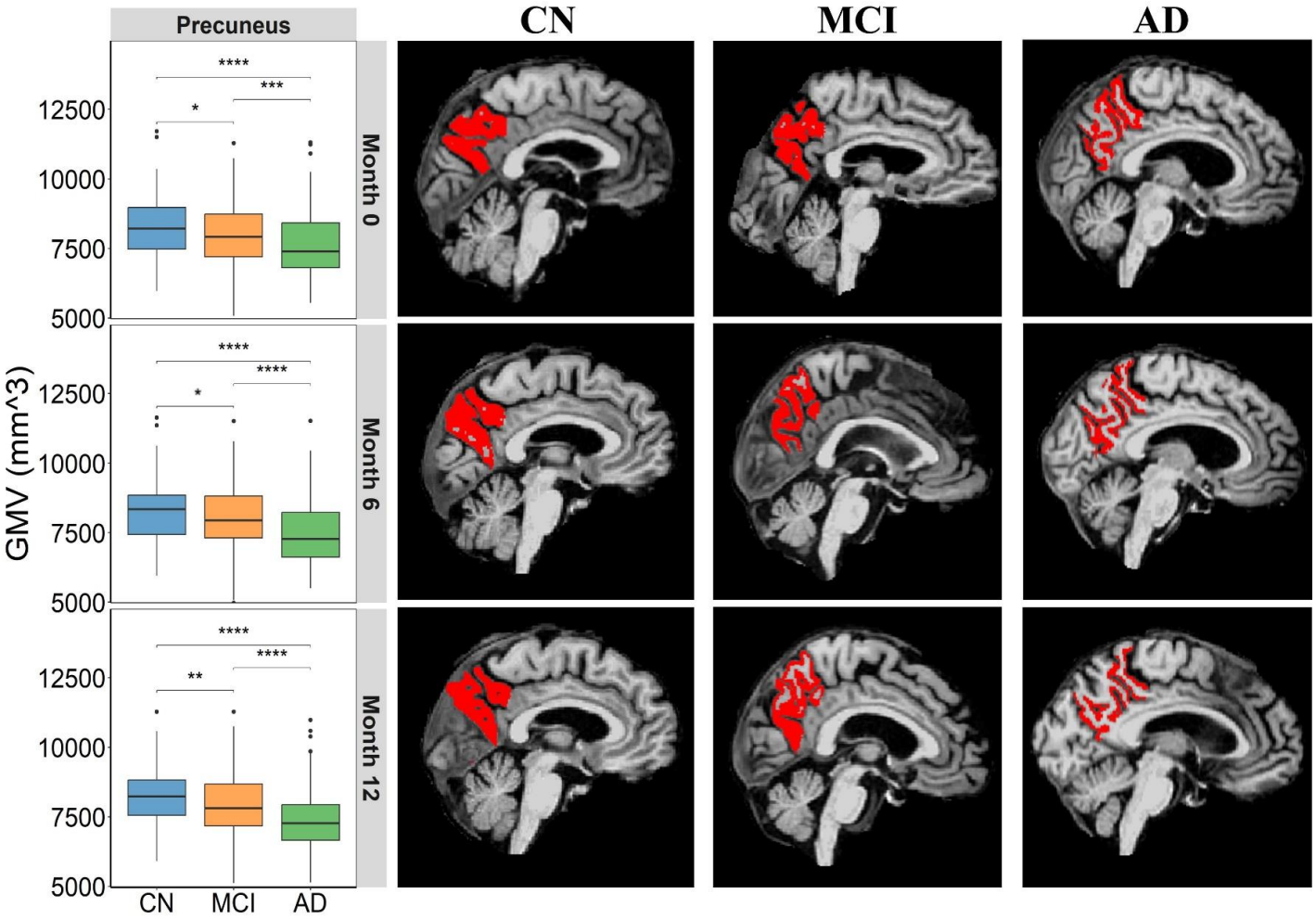

medRxiv preprint doi: https://doi.org/10.1101/2024.05.15.24307407; this version posted May 15, 2024. The copyright holder for this preprint (which was not certified by peer review) is the author/funder, who has granted medRxiv a license to display the preprint in perpetuity. It is made available under a CC-BY-NC-ND 4.0 International license .

Figure 3

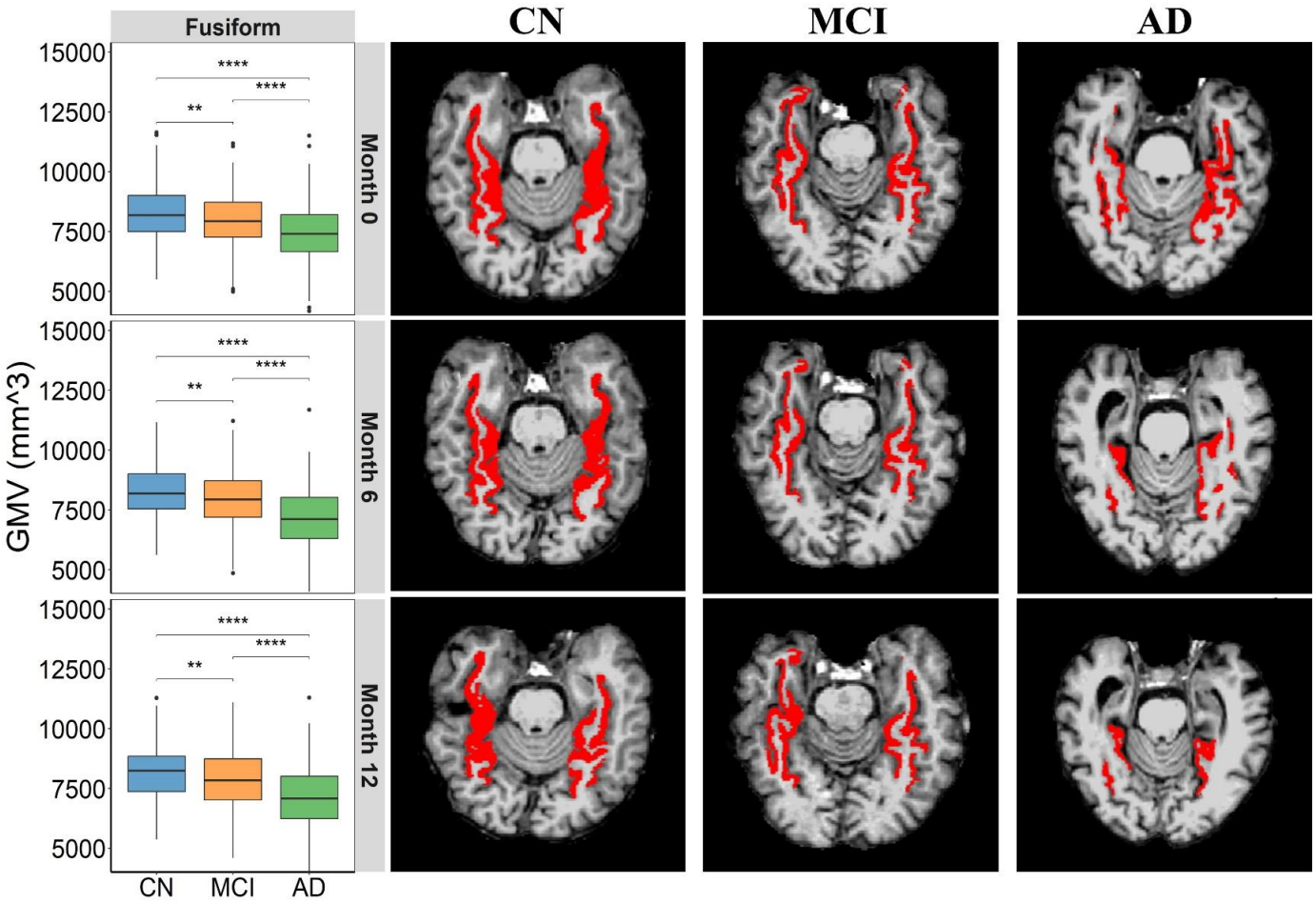

medRxiv preprint doi: https://doi.org/10.1101/2024.05.15.24307407; this version posted May 15, 2024. The copyright holder for this preprint (which was not certified by peer review) is the author/funder, who has granted medRxiv a license to display the preprint in perpetuity. It is made available under a CC-BY-NC-ND 4.0 International license .
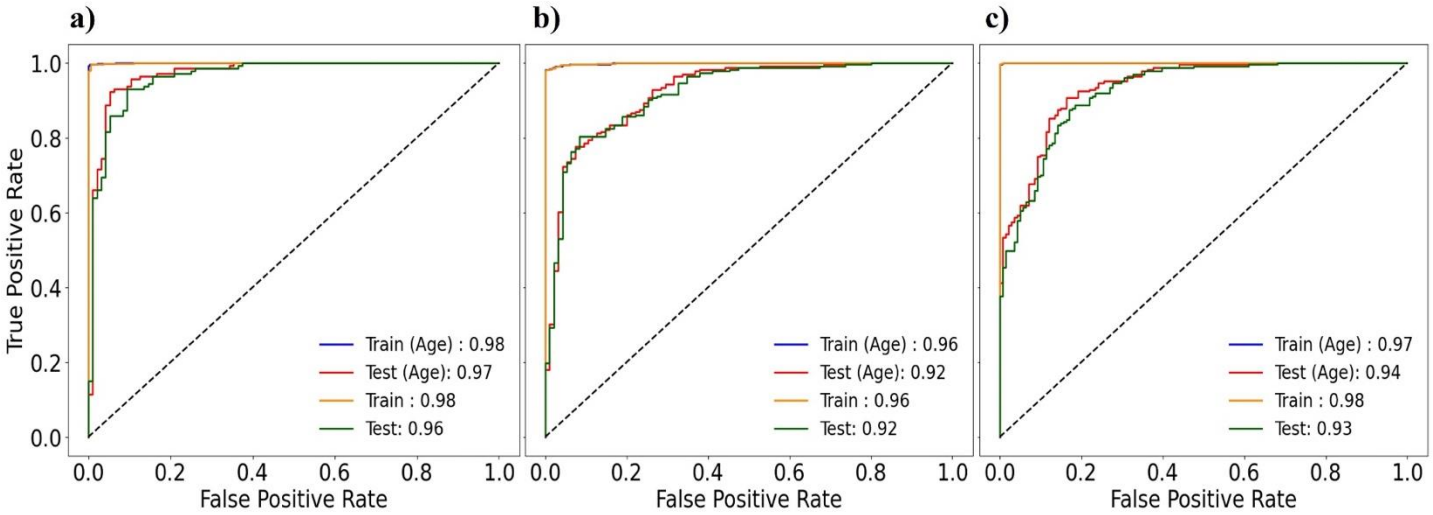
Figure 4